Plasmonic Mode Engineering with Templated Self-Assembled Nanoclusters

Plasmonic mode engineering with templated self-assembled nanoclusters

Jonathan A. Fan[1], Kui Bao[2], Li Sun[1], Jiming Bao[3], Vinothan N. Manoharan[1,4], Peter Nordlander[2], and Federico Capasso[1]

1. School of Engineering and Applied Sciences, Harvard University, 9 Oxford St, Cambridge MA 02138
2. Department of Physics, Rice University, 6100 Main St, Houston TX, 77005
3. Department of Electrical and Computer Engineering, University of Houston, Engineering Building 1, Houston TX, 77204
4. Department of Physics, Harvard University, 17 Oxford St, Cambridge MA, 02138

Keywords: plasmonics, templated self-assembly, Fano resonance, heptamer, magnetic dipole, nanoshell

Abstract

Plasmonic nanoparticle assemblies are a materials platform in which optical modes, resonant wavelengths, and near-field intensities can be specified by the number and position of nanoparticles in a cluster. A current challenge is to achieve clusters with higher yields and new types of shapes. In this Letter, we show that a broad range of plasmonic nanoshell nanoclusters can be assembled onto a lithographically-defined elastomeric substrate with relatively high yields using templated assembly. We assemble and measure the optical properties of three cluster types: Fano-resonant heptamers, linear chains, and rings of nanoparticles. The yield of heptamer clusters is measured to be over thirty percent. The assembly of plasmonic nanoclusters on an elastomer paves the way for new classes of plasmonic nanocircuits and colloidal metamaterials that can be transfer-printed onto various substrate mediums.

Metallic structures provide a bridge between electronics and photonics at the nanoscale because of their ability to support surface plasmons, which are oscillations of free electrons that couple with electromagnetic waves. Surface plasmons come in two flavors: surface plasmon polaritons, which couple to and propagate on the surface of metal films, and localized surface plasmons, which couple to metallic nanostructures. Self-assembled clusters of metal-dielectric nanoparticles provide a foundation for the latter because they are a basis for tunable plasmonic "molecules" that exhibit a broad range of resonances[1]. Electric resonances generally exist in all plasmonic clusters and can be tuned from the visible to infrared wavelengths in systems by modifying the size and shape of individual particles and their clusters[2]. Nanoparticles arranged in equilateral trimer[1] and other ring-like configurations[3] support magnetic dipole resonances perpendicular to the plane of the ring, and tetrahedral particle clusters support isotropic electric and magnetic resonances in three dimensions[4]. Fano-like resonances, which are characterized by a narrow dip in the scattering and extinction spectrum due to interference between two plasmonic modes[5-6], have been experimentally measured in hetero-dimer[7-8], asymmetric quadrumer[9], and symmetric heptamer[1] colloidal clusters.

In initial studies of nanoshell clusters exhibiting magnetic and Fano-like resonances, clusters were assembled randomly by capillary forces[1]. With this technique, close-packed clusters ranging from dimers and trimers to small aggregates were assembled, and the yield for any particular cluster type was small (few clusters per TEM grid). In addition, the clusters assembled at random positions on a substrate, and the only way to identify individual clusters was to examine the substrate over a wide area using electron microscopy. For applications requiring the bulk assembly of nanoclusters at

precisely defined locations, such as the fabrication of a metamaterial, more sophisticated self-assembly techniques are necessary.

We assemble gold nanoshells on a patterned elastomeric substrate by templated assembly. Nanoshells such as silica-core gold-shell particles[10] are sufficiently spherical to support controlled near-field optical coupling between packed adjacent particles. The templated assembly of these particles dramatically improves cluster yields and enables the assembly of non-close-packed structures, thereby expanding the scope of self-assembled plasmonic engineering. We note the precedent of previous studies in which clusters of large dielectric particles[11-12] and small metallic particles[13-15] were assembled with a template assembly process. However, resonances such as Fano-like resonances were not observed because the particles were too small and their faceting prevented controlled and reproducible interparticle near-field coupling. It is also noted that template-assembled silver aggregate clusters have been previously demonstrated to exhibit magnetic Mie modes[16-18]; however, these types of colloidal aggregates have limited tunability and cannot be generalized to support other types of resonances such as Fano resonances.

The assembly process is adapted from Ref. [19] and is summarized in Figure 1. The first step is the fabrication of the patterned substrate, which is accomplished by soft-lithography[20] (Figure 1a). Here, a silicon master consisting of a series of posts, which define the geometry of the voids on the substrate, is fabricated. The substrate itself is created by molding and curing a bilayer of hard Polydimethylsiloxane (h-PDMS, ~2μm-thick) and regular PDMS (~200μm-thick) on the silicon wafer, during which the silicon post patterns embed in the h-PDMS layer. The h-PDMS layer is used because it supports

pattern transfer with a spatial resolution down to 50nm, while the regular PDMS serves as a flexible elastomeric backing and improves the handling of the brittle h-PDMS[21]. The PDMS bilayer is then mounted on a glass slide, which serves as a rigid and transparent support.

To assemble particles onto the PDMS substrate, a concentrated solution of silica-gold nanoshells in water (~$3x10^{10}$/mL) is placed in an assembly shown in Figure 1b. Here, the droplet of particles is sandwiched between a glass slide and the substrate, which fixes the boundary of the droplet meniscus at the edge of the glass slide. The substrate, which is mounted on a motorized stage, is then moved slowly relative to the fixed glass slide, which draws the droplet meniscus across the substrate. As this meniscus moves over a PDMS void, nanoshells at the meniscus-substrate interface are pushed into the void by capillary forces. To pack the voids as fully as possible with particles, two additional parameters are controlled. One is the contact angle between the droplet and substrate, which sets the direction of capillary force on the nanoparticles (Figure 1b, inset). The second parameter is the substrate temperature, which sets the evaporation rate of the droplet at the meniscus. Droplet evaporation is necessary because it leads to the accumulation of nanoparticles at the meniscus-substrate interface[19] (Figure 1b, dotted line).

To optimize the cluster assembly process, nanoshells are assembled into cylindrical voids with different assembly parameters and cluster yields are examined using scanning electron microscopy (SEM). The nanoshells here have an average [r_1, r_2] = [63, 88] nm, where r_1 and r_2 are the inner core and total shell radii respectively, and they are functionalized with a thiolated poly(ethylene) glycol polymer, which serves as a

dielectric spacer between the packed nanoshells[1]. Heptamers are chosen as the target cluster, and substrates are patterned with cylindrical voids 140 nm deep and 580 nm in diameter to geometrically confine the assembled nanoparticles into heptamer configurations. Upon scanning the different assembly parameters, it was found that a droplet contact angle of approximately 25 degrees, substrate velocity of 0.6μm/sec, and substrate temperature of 21°C gave reasonably high heptamer yields. The contact angle is set by first oxygen plasma cleaning the PDMS, which makes it hydrophilic, and then waiting for the contact angle to slowly increase (time scale of hours). A representative SEM image of clusters assembled with these parameters is shown in Figure 2a, and many heptamer clusters are visible; a histogram of cluster distributions, created by examining 205 clusters, shows heptamer yields to be 32% (Figure 2b). The presence of smaller clusters can be addressed by starting with higher particle concentrations, better controlling the contact angle, and further optimizing the substrate speed and temperature.

With the processing parameters above, clusters are assembled on substrates comprising a range of void geometries, and optical scattering measurements are performed on individual clusters using a near-normal dark-field illumination technique described in Ref. [22]. Here, a 50x IR-corrected microscope objective with a numerical aperture of 0.65 is used to both focus incident radiation on the sample and collect scattered radiation. Dark-field illumination is accomplished by using a beam blocker to prevent incident light reflected from the substrate from entering the spectrometer. With this scheme, the incident light angle is set to 20 degrees. The reason why this technique is implemented, as oppose to dark-field schemes that utilize large incident angles[1], is to minimize background generated by the PDMS substrate itself; the PDMS substrates have

small bubbles and dielectric inclusions that scatter light, and the near-normal incidence scheme minimizes the collection of such light and enhances the signal-to-background ratio. This technique also minimizes the retarded excitation of the nanoclusters, which leads to "cleaner" spectra[22].

Scattering spectra of an individual heptamer cluster are shown in Figure 3, and the structure displays strong Fano-like resonances near 1370 nm for two different incident polarizations. Theoretical scattering spectra, calculated using the program COMSOL, are also shown in Figure 3, and they match well with the experimental plots. A further analysis of the bright and dark modes responsible for Fano interference can be found in the Supplementary Section. The matching Fano minimum wavelengths in the spectra for the two different polarizations indicate that the cluster is close-packed: as nanoshells fill the voids and the water completely evaporates, the nanoshells tightly pack together due to capillary forces. Deviations between the theoretical and experimental spectra are likely due to slight asymmetry in the experimental cluster, due to inhomogeneities in the nanoshell geometries. Unfortunately, limitations to electron microscopy make it is difficult to precisely identify nanoscale geometric aberrations in these clusters. Such inhomogeneities will be addressed in future work by starting with more uniform nanoshells for assembly, which can be achieved by growing nanoshells with more monodisperse silica cores and by using techniques such as density gradient centrifugation to purify nanoshell populations[23].

The peaks near 800nm in the experimental spectra are reproduced in the numerical spectra and appear to be due to scattering from the substrate void itself. The precise geometry used in the simulations is that of a truncated ellipsoid, and its geometry

is detailed in Figure 4a. The experimental realization of substrate voids with sloped, bowl-like walls is consistent with the soft lithography process, during which imperfect silicon master etching and mechanical relaxation of the elastomer after curing can contribute to a non-cylindrical void shape. The calculated scattering spectrum of this void with no nanoparticles shows a peak near 800nm (Figure 4b), indicating that the void is responsible for the peak in the heptamer spectra near 800nm. To further probe the dependence of the spectra on the precise shape of the void, simulated scattering spectra of the heptamer in the bowl-shaped void and a perfect cylinder are compared, and they are plotted in Figure 4c. Here, the spectrum of the heptamer in the perfectly cylindrical void displays no peak near 800nm; Mie scattering from the void itself appears to strongly depend on its exact geometry. Future research will focus on the precise optical properties of voids of different geometries and on the further characterization of experimentally fabricated substrates.

Nanoshell rings with three, four, and six nanoparticles are also assembled. Rings are of general interest because they support magnetic dipole modes[3], which are excited by the magnetic component of the electromagnetic field and are the basis for many metamaterial concepts. As discussed in Ref. [24], it is preferable to assemble rings consisting of a larger number of particles in the loop because in this limit, the magnetic dipole response becomes "purer:" the magnetic mode here is actually a magneto-electric hybrid mode comprising the magnetic dipole and other electric multipoles. The relative contributions of these electric multipoles diminish as the number of particles in the ring gets larger. Physically, this effect is related to the fact that the magnetic mode can be approximately described as a ring of electric dipoles, each supported by a particle and

oriented tangent to the ring. With fewer particles in the ring, the cumulative charge distributions of these electric dipoles resemble lower order electric multipolar ring modes (See Ref. [25] for examples of such charge distributions). As the number of particles increase, these charge distributions resemble higher order electric multipolar ring modes (i.e. hybridization with lower order multipoles is suppressed). Nanoshell trimers have been previously assembled by random capillary forces[1], but four and six particle rings are difficult to randomly assemble without a template because they are not close-packed structures. The six particle ring here forms by chance in a cylindrical void designed for heptamers; higher yields of these clusters can be achieved by fabricating substrate voids with ring-like shapes.

The spectra of all three ring types are presented in Figure 5 and feature a broad electric dipole peak that is isotropic in the plane of the clusters. These spectra match well with those numerically calculated. The six particle ring features a narrow peak near 800 nm, which is similar to that in the heptamer spectra and which is due to scattering from the substrate voids. The isotropy of these spectra is consistent with the group symmetries of the rings: all of these clusters have D_{nh} symmetry, where n is the number of particles in the ring, and structures with this symmetry generally support isotropic in-plane dipole resonances when n is 3 or greater[24].

This peak broadens as the number of particles in the rings increases largely because bigger rings have larger dipole moments, which leads to faster radiative decay and subsequent linewidth broadening. Additionally, it is suspected that part of the observed peak broadening is due to the presence of the magnetic dipole mode itself. A further numerical analysis of the quadrumer, presented in the Supplementary Section,

shows that the magnetic dipole mode can be directly excited with an incident light source at 20 degrees, and that it can be further enhanced by the presence of the dielectric void substrate; as such, the observed peak in the scattering spectra can be interpreted as the merging of the magnetic dipole with the electric dipole. Magnetic dipole measurements with a cross-polarizer[1] were attempted on these nanostructures, but unfortunately, magnetic dipole peaks could not be resolved because of noise caused by light scattering from the PDMS substrate itself. Future experiments will involve transfer printing these clusters to other planar substrates, which would eliminate these substrate-based issues.

Finally, linear chains of nanoshells comprising one to four particles are assembled in voids of varying length-to-width aspect ratio, and their spectra are plotted in Figure 6. The experimental and theoretical spectra agree well. Linear chains are of interest because they function as highly tunable electric dipole antennas, and longer chains are the basis for nanoscale energy transport[26]. The spectra of all of these structures are characterized by a broad dipole peak, and as the number of particles in the chain increases, these peaks red-shift from the visible to near-infrared wavelengths. The primary reason why the electric dipole resonance red-shifts with particle number is retardation effects, which arise when the size of the system becomes comparable to the excitation wavelength. The impact of retardation effects on red-shifting can be understood by examining simulations of nanoparticle chains near the quasi-static limit. In this regime, retardation effects are minimized; here, the spectra of the chains exhibit a significantly reduced electric dipole red-shift as a function of chain length[27]. In addition to retardation, the observed dipole red-shift is also due to increased capacitive coupling within the chains. This phenomenon can be explained by the nanocircuit model developed by Engheta and Alu[28], in which

subwavelength metal and dielectric features in a nanostructure are modeled as nanoinductors and nanocapacitors, respectively. As additional particles are added to the chain, additional capacitive interactions at the interparticle gaps are formed. This capacitance is described by the strong attractive Coulomb interaction between free surface charges on adjacent particles and is characterized by a large field intensity, or hot spot, within these gaps[29]. This enhanced total capacitance contributes a red-shifting of the nanoshell chain electric dipole.

The ordered assembly of plasmonic nanoclusters on substrates provides a foundation for a broad range of new applications. One is the bulk assembly of magnetic and Fano-resonant clusters, and more generally, the construction of self-assembled metamaterials. What is particularly exciting is the potential to assemble three-dimensional structures such as tetrahedral clusters[11], which are building blocks for isotropic magnetic and negative-index materials[4], and new types of waveguides[30]. It is also noted that the substrate patterning is not limited to periodic features but can include arbitrary patterns, and as such, this assembly technique can be applied to construct new types of self-assembled optical nanocircuits integrating phase elements[31], optical antennas, waveguides, filters, and other optical components.

The assembly of plasmonic materials specifically on elastomeric substrates supports features not found in conventional lithographically-defined nanostructure engineering. One feature is the possibly to stretch and reconfigure the plasmonic nanostructures on the substrate surface by stretching the elastomer[32-33], which can lead to a new regime of mechanically tunable optical materials. Another feature is the transfer printing of clusters onto other arbitrary substrates. These printing techniques have been

developed for single nanoparticles[14] and for other semiconducting and dielectric microstructures[34], and they provide a route to integrating self-assembled plasmonic structures with other types of materials.

In conclusion, we have shown that the self-assembly of nanoparticles on a templated substrate is an efficient method for the large scale fabrication of nanoparticle clusters. By varying the size and shape of the voids in the template, it is possible to control the geometry of the individual clusters and thus to engineer specific optical modes such as magnetic and Fano resonances. By combining the top-down fabrication of substrates with the bottom-up assembly of nanoclusters, new hybrid materials can be created with exciting potential in a wide range of optical materials engineering applications.

Acknowledgements

Electron microscopy was performed at the Center for Nanoscale Science at Harvard University, a member of the National Nanotechnology Infrastructure Network. J. A. F. and F. C. acknowledge the NSF Nanoscale Science and Engineering Center (NSEC). J. A. F. acknowledges Y. Cao for simulation support, Q. Zhang, Z. Liu, and X. Lu for assisting with experiments, M. Barber for initial substrate prototyping, and Y. Yin, T. Kraus, and M. Kats for helpful discussions. P.N. and K. B. acknowledges support from the Robert A. Welch foundation (C-1222), the US Department of Defense NSEFF program (N00244-09-1-0067), and the Office of Naval Research (N00244-09-1-0989). J. M. B. acknowledges support from the Robert A. Welch Foundation (E-1728).

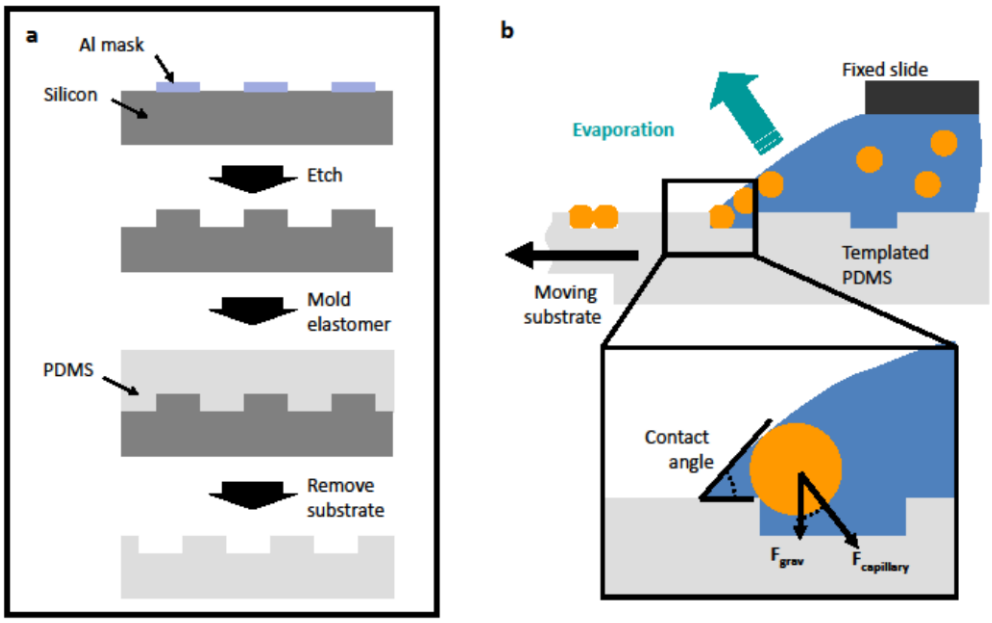

Figure 1. Schematics of the templated assembly of nanoshell clusters. a, To create the PDMS substrates, a silicon master is fabricated: electron beam lithography defines the post geometries on the wafer, aluminum is deposited as an etch mask, silicon posts are dry-etched, and the silicon is functionalized with a fluorinated polymer to prevent PDMS adhesion. A bilayer of h-PDMS and regular PDMS is then cured on top of the silicon master, peeled off, and mounted to a glass piece. **b,** Nanoshells are packed into the PDMS voids by sandwiching a water droplet with particles between the substrate and a glass slide and then moving the droplet meniscus across the substrate. During this process, particles are pushed into the voids via capillary forces (inset). The substrate speed, temperature, and droplet-substrate contact angle are controlled to optimize the clustering process.

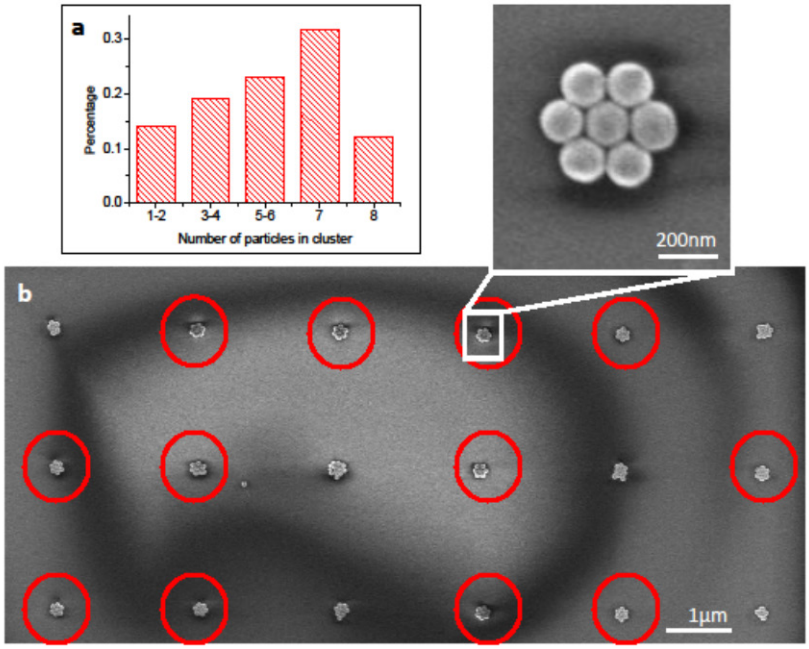

Figure 2. Image of assembled heptamers. a, Histogram of the distribution of clusters assembled on the PDMS template. Heptamers are assembled with 32% yield. The presence of many smaller clusters suggests that particle packing is limited by low nanoshell concentrations, and that increasing these concentrations can improve yields. **b,** SEM image of an array of heptamers assembled on a PDMS template. The heptamers are circled; other types of clusters also are visible due to the stochastic nature of the assembly process. The inset shows a detailed image of an individual heptamer and shows that the cluster is close-packed.

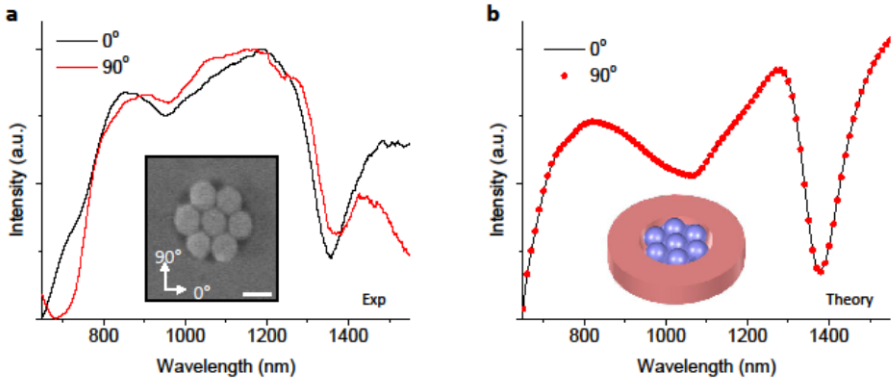

Figure 3. Images and spectra of a heptamer cluster. a, Spectra of a single symmetric heptamer, assembled using the template geometry featured in Figure 2a, displays an isotropic Fano-like resonance near 1350 nm. The polarization directions of the incident beams are defined in the SEM image. The scale bar in the SEM images is 200nm. **b,** Numerical spectra of the heptamer agree well with the experimental spectra in (a).

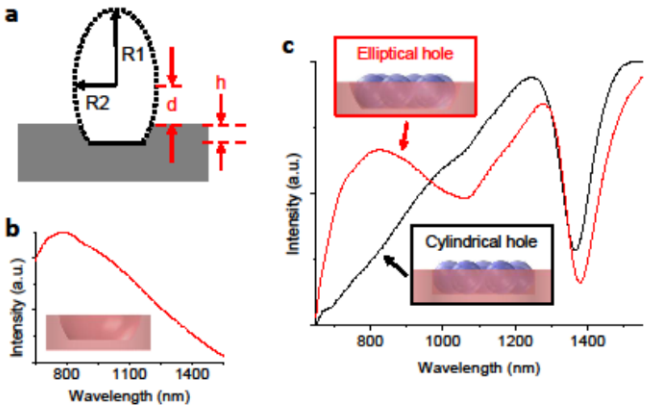

Figure 4. Void modeling and its effect on spectra. a, The elliptical void geometry is defined in the substrate (gray) by an ellipsoid, shown in cross-section (dotted curve). Its center is offset above the substrate by the distance d. The bottom of the void is subsequently flattened at the depth h. **b,** Simulated scattering spectrum of an elliptical substrate void with a geometry matching that used in Figure 3. **c,** Simulated scattering spectra of a heptamer in a cylindrical and elliptical void. The parameters used in the simulation match those from Figure 3.

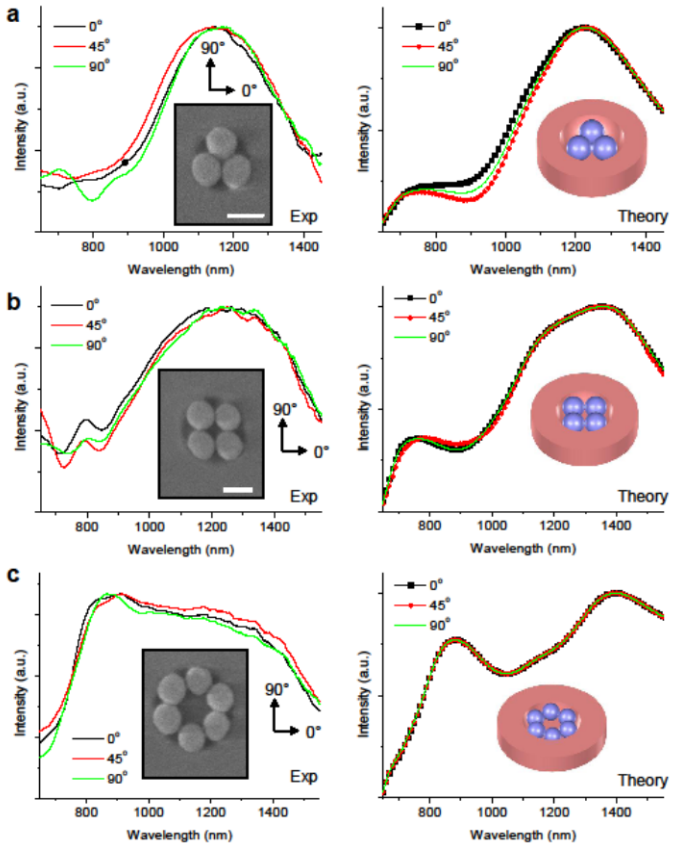

Figure 5. Images and spectra of nanoshell rings. Spectra and SEM images of **a,** three particle, **b,** four particle, and **c,** six particle rings are presented for different polarization orientations of the incident light. The number of particles in the ring is determined by the size of the circular void. All of these clusters display isotropic in-plane electric dipole resonances due to their high degree of symmetry.

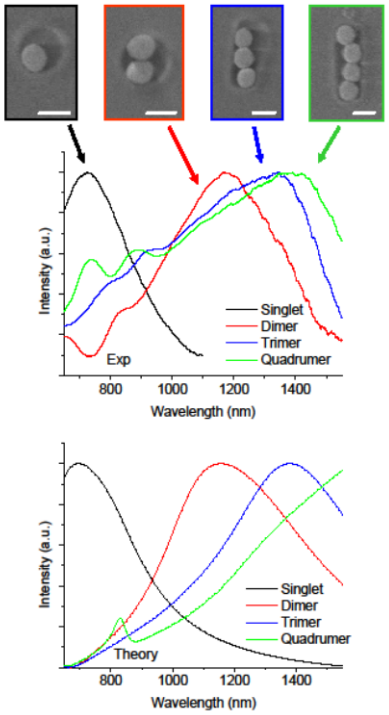

Figure 6. Images and spectra of linear chains of nanoshells. Linear chains of nanoshells are assembled by using substrate voids with different aspect ratios. As the number of particles in the chain increases, the electric dipole resonance peak experiences a red-shift due to enhanced capacitive coupling between the nanoparticles in the cluster. The theoretical spectra of these nanoshell chains show the same red-shifting behavior.

References

1 Fan, J. A. *et al.* Self-Assembled Plasmonic Nanoparticle Clusters. *Science* **328**, 1135-1138, doi:10.1126/science.1187949 (2010).

2 Lal, S., Link, S. & Halas, N. J. Nano-optics from sensing to waveguiding. *Nat. Photonics* **1**, 641-648, doi:10.1038/nphoton.2007.223 (2007).

3 Alu, A., Salandrino, A. & Engheta, N. Negative effective permeability and left-handed materials at optical frequencies. *Opt. Express* **14**, 1557-1567 (2006).

4 Urzhumov, Y. A. *et al.* Plasmonic nanoclusters: a path towards negative-index metafluids. *Opt. Express* **15**, 14129-14145 (2007).

5 Luk'yanchuk, B. *et al.* The Fano resonance in plasmonic nanostructures and metamaterials. *Nat Materials* **9**, 707-715 (2010).

6 Liu, N. *et al.* Plasmonic analogue of electromagnetically induced transparency at the Drude damping limit. *Nature Materials* **8**, 758-762, doi:http://www.nature.com/nmat/journal/v8/n9/suppinfo/nmat2495_S1.html (2009).

7 Brown, L. V., Sobhani, H., Lassiter, J. B., Nordlander, P. & Halas, N. J. Heterodimers: Plasmonic Properties of Mismatched Nanoparticle Pairs. *ACS Nano* **4**, 819-832, doi:10.1021/nn9017312 (2010).

8 Bachelier, G. *et al.* Fano Profiles Induced by Near-Field Coupling in Heterogeneous Dimers of Gold and Silver Nanoparticles. *Physical Review Letters* **101**, doi:197401
10.1103/PhysRevLett.101.197401 (2008).

9 Fan, J. A. *et al.* Fano-like Interference in Self-Assembled Plasmonic Ouadrumer Clusters. *Nano Lett.* **10**, 4680-4685, doi:10.1021/nl1029732 (2010).

10 Oldenburg, S. J., Averitt, R. D., Westcott, S. L. & Halas, N. J. Nanoengineering of optical resonances. *Chem. Phys. Lett.* **288**, 243-247 (1998).

11 Yin, Y. D., Lu, Y., Gates, B. & Xia, Y. N. Template-assisted self-assembly: A practical route to complex aggregates of monodispersed colloids with well-defined sizes, shapes, and structures. *J. Am. Chem. Soc.* **123**, 8718-8729, doi:10.1021/ja011048v (2001).

12 Yin, Y. D., Lu, Y. & Xia, Y. N. A self-assembly approach to the formation of asymmetric dimers from monodispersed spherical colloids. *J. Am. Chem. Soc.* **123**, 771-772, doi:10.1021/ja0031873 (2001).

13 Cui, Y. *et al.* Integration of colloidal nanocrystals into lithographically patterned devices. *Nano Lett.* **4**, 1093-1098, doi:10.1021/nl049488i (2004).

14 Kraus, T. *et al.* Nanoparticle printing with single-particle resolution. *Nat. Nanotechnol.* **2**, 570-576, doi:10.1038/nnano.2007.262 (2007).

15 Yan, B. *et al.* Engineered SERS Substrates With Multiscale Signal Enhancement: Nanoplarticle Cluster Arrays. *ACS Nano* **3**, 1190-1202, doi:10.1021/nn800836f (2009).

16 Tamma, V. A., Lee, J. H., Wu, Q. & Park, W. Visible frequency magnetic activity in silver nanocluster metamaterial. *Appl. Optics* **49**, A11-A17 (2010).

17 Muhlig, S. *et al.* Optical properties of a fabricated self-assembled bottom-up bulk metamaterial. *Opt. Express* **19**, 9607-9616 (2011).
18 Wheeler, M. S., Aitchison, J. S., Chen, J. I. L., Ozin, G. A. & Mojahedi, M. Infrared magnetic response in a random silicon carbide micropowder. *Physical Review B* **79**, doi:073103
10.1103/PhysRevB.79.073103 (2009).
19 Malaquin, L., Kraus, T., Schmid, H., Delamarche, E. & Wolf, H. Controlled particle placement through convective and capillary assembly. *Langmuir* **23**, 11513-11521, doi:10.1021/la700852c (2007).
20 Xia, Y. N. & Whitesides, G. M. Soft lithography. *Annu. Rev. Mater. Sci.* **28**, 153-184, doi:10.1146/annurev.matsci.28.1.153 (1998).
21 Odom, T. W., Love, J. C., Wolfe, D. B., Paul, K. E. & Whitesides, G. M. Improved pattern transfer in soft lithography using composite stamps. *Langmuir* **18**, 5314-5320, doi:10.1021/la020169l (2002).
22 Fan, J. A. *et al.* Near-Normal Incidence Dark-Field Microscopy: Applications to Nanoplasmonic Spectroscopy. *Nano Lett.* **12**, 2817-2821, doi:10.1021/nl300160y (2012).
23 Carney, R. P. *et al.* Determination of nanoparticle size distribution together with density or molecular weight by 2D analytical ultracentrifugation. *Nat Commun* **2**, 335, doi:http://www.nature.com/ncomms/journal/v2/n6/suppinfo/ncomms1338_S1.html (2011).
24 Alu, A. & Engheta, N. Dynamical theory of artificial optical magnetism produced by rings of plasmonic nanoparticles. *Physical Review B* **78**, doi:085112
10.1103/PhysRevB.78.085112 (2008).
25 Hao, F., Larsson, E. M., Ali, T. A., Sutherland, D. S. & Nordlander, P. Shedding light on dark plasmons in gold nanorings. *Chem. Phys. Lett.* **458**, 262-266, doi:10.1016/j.cplett.2008.04.126 (2008).
26 Maier, S. A. & Atwater, H. A. Plasmonics: Localization and guiding of electromagnetic energy in metal/dielectric structures. *Journal of Applied Physics* **98**, doi:011101
10.1063/1.1951057 (2005).
27 Slaughter, L. S. *et al.* Towards Plasmonic Polymers. *Nano Lett.* **Accepted** (2012).
28 Engheta, N. Circuits with light at nanoscales: Optical nanocircuits inspired by metamaterials. *Science* **317**, 1698-1702, doi:10.1126/science.1133268 (2007).
29 Nordlander, P., Oubre, C., Prodan, E., Li, K. & Stockman, M. I. Plasmon hybridizaton in nanoparticle dimers. *Nano Lett.* **4**, 899-903, doi:10.1021/nl049681c (2004).
30 Yin, Y. & Xia, Y. Self-Assembly of Spherical Colloids into Helical Chains with Well-Controlled Handedness. *J. Am. Chem. Soc.* **125**, 2048-2049, doi:10.1021/ja029408h (2003).
31 Yu, N. *et al.* Light Propagation with Phase Discontinuities: Generalized Laws of Reflection and Refraction. *Science* **334**, 333-337, doi:10.1126/science.1210713 (2011).

32 Pryce, I. M., Aydin, K., Kelaita, Y. A., Briggs, R. M. & Atwater, H. A. Highly Strained Compliant Optical Metamaterials with Large Frequency Tunability. *Nano Lett.* **10**, 4222-4227, doi:10.1021/nl102684x (2010).
33 Yan, X. *et al.* Fabrication of non-close-packed arrays of colloidal spheres by soft lithography. *J. Am. Chem. Soc.* **127**, 7688-7689, doi:10.1021/ja0428208 (2005).
34 Sun, Y. G. & Rogers, J. A. Inorganic semiconductors for flexible electronics. *Adv. Mater.* **19**, 1897-1916, doi:10.1002/adma.200602223 (2007).

Supplementary Section for "Plasmonic mode engineering with templated self-assembled nanoclusters"

Jonathan A. Fan[1], Kui Bao[2], Li Sun[1], Jiming Bao[3], Vinothan N. Manoharan[1,4], Peter Nordlander[2], and Federico Capasso[1]

1. School of Engineering and Applied Sciences, Harvard University, 9 Oxford St, Cambridge MA 02138
2. Department of Physics, Rice University, 6100 Main St, Houston TX, 77005
3. Department of Electrical and Computer Engineering, University of Houston, Engineering Building 1, Houston TX, 77204
4. Department of Physics, Harvard University, 17 Oxford St, Cambridge MA, 02138

Simulation Parameters

For all simulations, the incident beam is defined as a plane wave with an incidence angle 20 degrees from the normal to the sample surface, and scattered radiation is collected from a solid angle defined by the numerical aperture of 0.65. The nanoshell dimensions are defined to be $[r_1, r_2] = [62.5\ 92.5]$nm with interparticle gap separations of 2nm. These gaps are filled with a dielectric of permittivity $\varepsilon = 2.09$. The substrate consists of a dielectric with $\varepsilon = 2.25$. The substrate void parameters for different clusters are the following:

--For trimers, d = 55.0nm and R1 = R2 = 240.5nm

--For quadrumers, d = 20.2 nm and R1 = R2 = 240.5nm

--For hexamers and heptamers, d = 158.7 nm, R1 = 632.4nm, and R2 = 306.9nm

The voids used for linear nanoshell chains are all rectangular.

Heptamer cluster analysis

The nature of the bright and dark modes featured in the heptamer in Figure 3 can be elucidated by examining the surface charge distributions of the modes. We plot the charge distributions of the heptamer bright mode (1500nm) and dark mode (1370nm) in Figure 1Sa, together with the extinction and absorption spectra of the cluster. The geometry of the simulated system here is identical to that in Figure 3 except for the angle of incident polarization, which is selected to be 45 degrees for clarity of the surface charge profiles. The dark mode charge distribution shows that the dipoles of the individual nanoshells (white arrows) are oriented in different directions, such that the overall dipole moment of the cluster is small. The bright mode charge distribution shows that the dipoles of the individual nanoshells are generally oriented in

the same direction, such that the overall dipole moment of the cluster is large. This analysis is consistent with that in Ref. [1]; there exist small discrepancies between the charge distributions here compared to those in Ref. [1] due to substrate effects and to the use of a different incidence angle.

We also extend our analysis of Figure 4 by plotting the extinction spectrum of the heptamer with and without the elliptical void substrate from 700-2000nm. Here, we can see that with the presence of the substrate, there exists a strong enhancement of the magnetic dipole mode, suggesting some level hybridization of the magnetic and electric dipole modes due to symmetry breaking by the substrate.

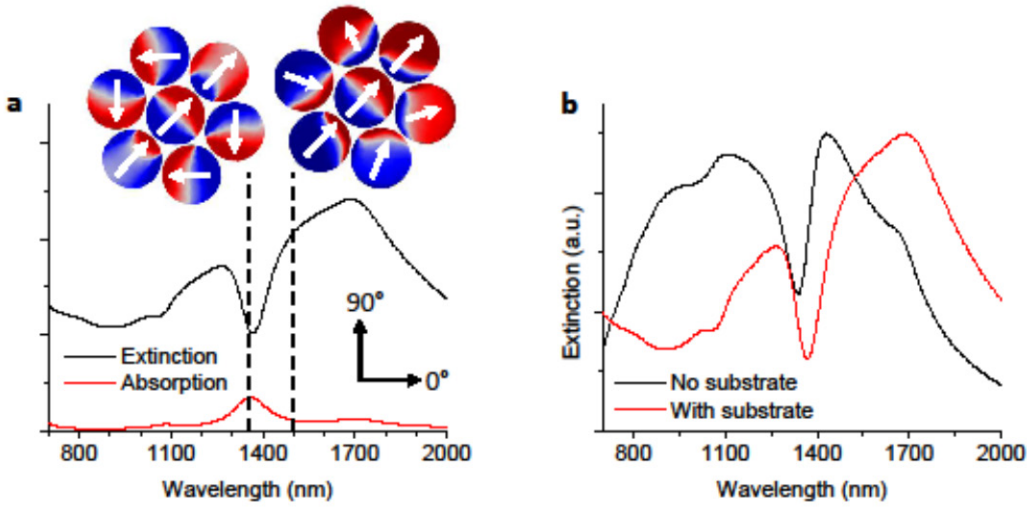

Figure 1S. Numerical heptamer cluster analysis. (a) Extinction and absorption spectra of the heptamer cluster modeled in Figure 3, with s-polarized incident light, an incidence angle of 20 degrees, and a polarization orientation of 45 degrees (axes defined in the figure). Surface charge distributions of the bright (1500nm) and dark modes (1370nm) are plotted. **(b)** Extinction spectra of the heptmer with and without the substrate.

Quadrumer cluster analysis

The broad "dipole peaks" in the quadrumer scattering spectra in Figure 5 are further analyzed by examining surface charge distributions of the cluster at different frequencies. We plot the charge distributions of the quadrumer at 1200nm (near the peak of the "dipole peak") and 1390nm (at the edge of the "dipole peak") in Figure 2Sa, together with the extinction and absorption spectra of the cluster. The simulation parameters here are identical to those used in Figure 5. Unlike the scattering spectra in Figure 5, where the "dipole peak" appears as a single broad peak, these extinction and absorption spectra show a distinct peak near 1390nm. The charge distribution at 1200nm shows that the dipoles of the individual nanoshells are generally oriented in the same direction, such that the overall dipole moment of the cluster is large. This indicates that this is the bright electric dipole mode. The charge distribution at 1390nm shows that the dipoles of the individual nanoshells are oriented in a ring; together with the narrow and distinct peak in the absorption spectrum, this indicates the presence of a magnetic dipole mode. Similar to the magnetic trimer mode in Ref. [1], the magnetic mode here is red-shifted beyond the peak of the electric dipole mode due to particularly strong capacitive coupling between neighboring nanoshells.

To further analyze the origin of the observed magnetic dipole peak, we calculate the extinction spectrum of the quadrumer with different incidence angles and substrate conditions (Figure 2Sb). For the case of no substrate and normal incidence, we see a broad electric dipole and no magnetic dipole peak in the spectrum (black line), indicating that the magnetic dipole is not getting excited. This is consistent with the fact that the incident light here has no magnetic field component that is normal to the ring of particles. If the incident light angle is set to 20 degrees, a small magnetic dipole peak emerges (red line, near 1380nm), due to the presence of a small magnetic field component normal to the cluster. Finally, if the dielectric void substrate is

added, the magnetic dipole is further enhanced (green line), due to hybridization between the magnetic and electric dipole modes, which is mediated by symmetry breaking caused by the substrate. This is consistent with the magneto-electric coupling observed in Figure 1S.

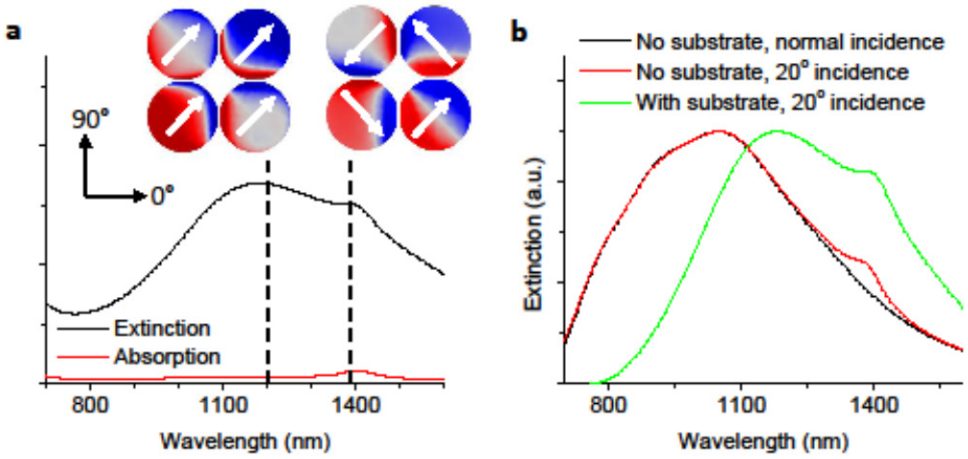

Figure 2S. Numerical quadrumer cluster analysis. (a) Extinction and absorption spectra of the quadrumer cluster modeled in Figure 5, with s-polarized incident light, an incidence angle of 20 degrees, and a polarization orientation of 45 degrees (axes defined in the figure). Surface charge distributions of the electric dipole mode (1200nm) and the magnetic dipole mode (1390nm) are plotted. **(b)** Extinction spectra of the quadrumer with different incidence angles and substrate conditions.